

Article

Carbon Nitride-Perovskite Composites: Evaluation and Optimization of Photocatalytic Hydrogen Evolution in Saccharides Aqueous Solution

Andrea Speltini ^{1,*}, Lidia Romani ², Daniele Dondi ², Lorenzo Malavasi ² and Antonella Profumo ^{2,*}

¹ Department of Drug Sciences, University of Pavia, via Taramelli 12, 27100 Pavia, Italy

² Department of Chemistry, University of Pavia, via Taramelli 12, 27100 Pavia, Italy;

lidia.romani01@universitadipavia.it (L.R.); daniele.dondi@unipv.it (D.D.); lorenzo.malavasi@unipv.it (L.M.)

* Correspondence: andrea.speltini@unipv.it (A.S.); antonella.profumo@unipv.it (A.P.);

Tel.: +39-0382-987349 (A.S.)

Received: 29 September 2020; Accepted: 29 October 2020; Published: 30 October 2020



Abstract: The application of hybrid photocatalysts made of carbon nitride and lead-free perovskites, namely $\text{DMASnBr}_3/\text{g-C}_3\text{N}_4$ and $\text{PEA}_2\text{SnBr}_4/\text{g-C}_3\text{N}_4$, for the H_2 evolution from saccharides aqueous solution is described. The novel composites were tested and compared in terms of hydrogen evolution rate (HER) under simulated solar light, using Pt as a reference co-catalyst, and glucose as a representative sacrificial biomass. The conditions were optimized to maximize H_2 generation by a design of experiments involving catalyst amount, glucose concentration and Pt loading. For both materials, such parameters affected significantly H_2 photogeneration, with the best performance observed using 0.5 g L^{-1} catalyst, 0.2 M glucose and 0.5 wt\% Pt . Under optimized conditions, $\text{DMASnBr}_3/\text{g-C}_3\text{N}_4$ showed a 5-fold higher HER compared to $\text{PEA}_2\text{SnBr}_4/\text{g-C}_3\text{N}_4$, i.e., $925 \mu\text{moles g}^{-1} \text{ h}^{-1}$ and $190 \mu\text{moles g}^{-1} \text{ h}^{-1}$, respectively ($\text{RSD} \leq 11\%$, $n = 4$). The former composite, which affords an HER 15-fold higher in aqueous glucose than in neat water, provided H_2 also with no metal co-catalyst (around $140 \mu\text{moles g}^{-1} \text{ h}^{-1}$), and it was reusable for at least three photoreactions. Encouraging results were also collected by explorative tests on raw starch solution (around $150 \mu\text{moles g}^{-1} \text{ h}^{-1}$).

Keywords: hydrogen; catalyst; photocatalysis; biomass; solar light; perovskite; carbon nitride; design of experiments

1. Introduction

The search for new photocatalytic systems working under solar light for hydrogen production is increasingly triggering the interest of the scientific community. In the framework of novel photocatalysts, graphitic carbon nitride ($\text{g-C}_3\text{N}_4$) has emerged in the last decade as one of the most promising material to run H_2 photoproduction from water under visible light, due to cost-effective and easy synthesis, chemical stability, narrow band-gap and band potentials suitable to perform relevant redox reactions in aqueous solution [1,2]. Its intrinsic limitations, namely relatively high charge carriers recombination, low surface area and restricted light harvesting in the visible region, have been in part compensated by several strategies. For instance, metal and non-metal doping, structural and morphological modifications, dye-sensitization, and combination with co-catalysts of different nature (e.g., carbon nanotubes, carbon dots, bimetallic deposition) have proved to be rewarding in terms of enhanced photocatalytic activity towards H_2 generation from water also in the presence of sacrificial agents [2,3]. Among these, mainly fine chemicals have been used, as recently reviewed by Nasir et al. [2], while just a few studies were undertaken in aqueous biomass solutions or directly in wastewaters [4–6].

In recent times, the application of metal halide perovskites (MHPs) in the photocatalysis field has aroused great interest in view of the relatively narrow bandgaps compared to traditional metal oxide photocatalysts [7,8]. MHPs possess exclusive optical properties, viz. consistent light absorption in the visible region, tunable band-gap and extended carriers lifetimes, conveniently exploited in photovoltaics and optoelectronics [9].

Recently, coupling MHPs with $g\text{-C}_3\text{N}_4$ has become a cutting-edge research field [2,10,11], although limited work has been done so far concerning photocatalysis [2]. Recently, lead-free MHPs showing an exceptional stability in water were synthesized and characterized [12–14], thus opening a new avenue for the preparation and application of innovative photocatalysts. In this context, our group advantageously coupled dimethylammonium and phenylethylammonium-based perovskites— DMASnBr_3 and $\text{PEA}_2\text{SnBr}_4$, respectively—to $g\text{-C}_3\text{N}_4$, providing new micro-sized composites with excellent photocatalytic properties towards H_2 production from triethanolamine (TEOA) aqueous solution; in particular, up to a 20-fold increase of hydrogen evolution rate (HER) was achieved compared to $g\text{-C}_3\text{N}_4$ alone, due to a synergistic effect between the two constituents in the composite [12,13], essentially due to improved charge carrier separation. Such an effect results from the positive band-alignment between the two semiconductors, namely the MHP and $g\text{-C}_3\text{N}_4$, and the perovskite is selected based on its bandgap in order to exploit this synergistic effect. It was also observed in an explorative test that such catalytic systems are capable of generating H_2 from glucose solution under UV-visible light, with HERs from 30 to 100 times higher relative to pristine $g\text{-C}_3\text{N}_4$ [12,13].

In this study, the two best performing materials we previously identified, namely 5% $\text{PEA}_2\text{SnBr}_4/g\text{-C}_3\text{N}_4$ and 33% $\text{DMA}\text{SnBr}_3/g\text{-C}_3\text{N}_4$, were systematically tested, under simulated solar light, in aqueous glucose through a design of experiments (DoE) with the aim to maximize HER and compare the performance of each photocatalyst under the best conditions. The most performant composite was further investigated for its photo-chemical stability by recycling tests, compared to the well-known Evonik Aeroxide[®] P25 TiO_2 , used without any metal co-catalyst, and in the presence of soluble starch as a low-cost and abundant polysaccharide.

2. Results and Discussion

Based on the preliminary findings obtained with carbon nitride-perovskite composites in TEOA solution [12,13], the two best performing materials, 33% $\text{DMA}\text{SnBr}_3/g\text{-C}_3\text{N}_4$ and 5% $\text{PEA}_2\text{SnBr}_4/g\text{-C}_3\text{N}_4$, are investigated here for a systematic study of H_2 photoproduction from glucose aqueous solution. Glucose was selected as a biomass-derived sacrificial agent because in the wastewaters from food industry sugars are present at considerable amounts [4,5], and Pt was used as the reference metal co-catalyst because of its excellent properties for water reduction due to the large work function, resulting in a strong Schottky barrier effect [15,16].

2.1. Comparison between $\text{DMA}\text{SnBr}_3/g\text{-C}_3\text{N}_4$ and $\text{PEA}_2\text{SnBr}_4/g\text{-C}_3\text{N}_4$ after Chemometric Optimization

With the aim of investigating the behavior of the two catalysts and maximizing H_2 evolution, a chemometric approach was chosen to easily individuate the effects of the key operational parameters of heterogeneous photocatalysis, namely the relative amounts of catalyst, glucose and metal [17–20]. Accordingly, a full 2^3 experimental design was setup considering glucose concentration (x_1), catalyst amount (x_2) and Pt loading (x_3). As reported in Table 1, the experimental domain was comprised of two levels (−1 and +1) of each variable.

Table 1. Experimental domain for the 2³ factorial design.

Variable	Level Codes	
	−1	+1
Glucose concentration (M), x_1	0.025	0.2
Catalyst amount (g L ^{−1}), x_2	0.5	2
Pt loading (wt%), x_3	0.5	3

HERs obtained under the different conditions (mean values of duplicate tests), according to the experimental matrix, are reported in Table 2.

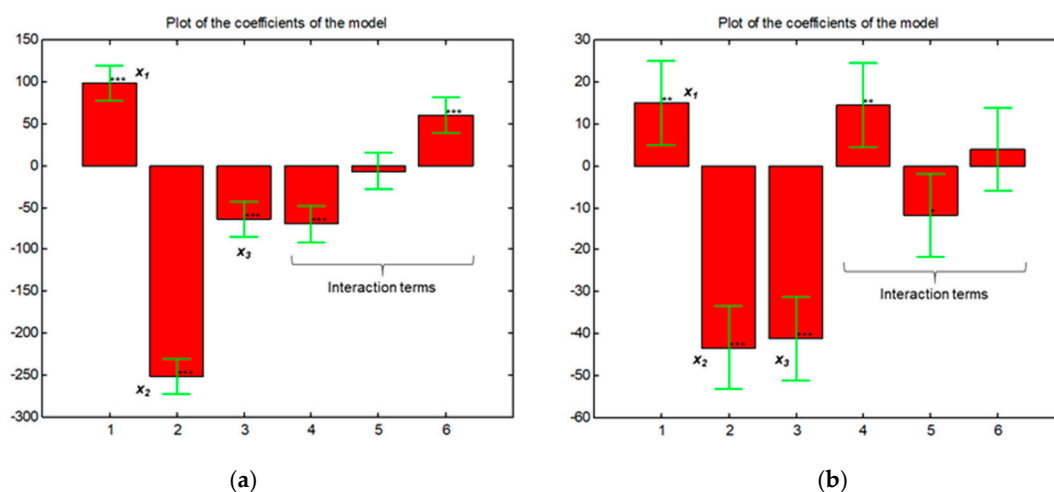
Table 2. Mean hydrogen evolution rates (HERs) obtained in the conditions of the experimental plan for both composite photocatalysts.

Exp	Glucose Concentration (M), x_1	Catalyst Amount (g L ^{−1}), x_2	Pt Loading (wt%), x_3	DMA ₂ SnBr ₃ /g-C ₃ N ₄ HER (μmoles g ^{−1} h ^{−1})	PEA ₂ SnBr ₄ /g-C ₃ N ₄ HER (μmoles g ^{−1} h ^{−1})
1	0.2	2	3	143	27
2	0.025	2	3	128	14
3	0.2	0.5	3	696	99
4	0.025	0.5	3	341	100
5	0.2	2	0.5	194	147
6	0.025	2	0.5	92	43
7	0.2	0.5	0.5	925	191
8	0.025	0.5	0.5	606	188

The values were used as the experimental response (y), and they were modeled (Matlab[®] software) relative to each variable (x_i), in line with the following equation:

$$y = b_0 + b_1x_1 + b_2x_2 + b_3x_3 + b_{12}x_1x_2 + b_{13}x_1x_3 + b_{23}x_2x_3, \quad (1)$$

Figure 1 shows the plot of the coefficients (b_i) of the model, while the response surfaces are gathered in Figure 2.

**Figure 1.** Plots of the coefficients of the model for (a) DMA₂SnBr₃/g-C₃N₄ and (b) PEA₂SnBr₄/g-C₃N₄. Stars indicate the significance of the coefficients (* $p < 0.05$, ** $p < 0.01$, *** $p < 0.001$), while error bars indicate the confidence intervals ($p = 0.05$).

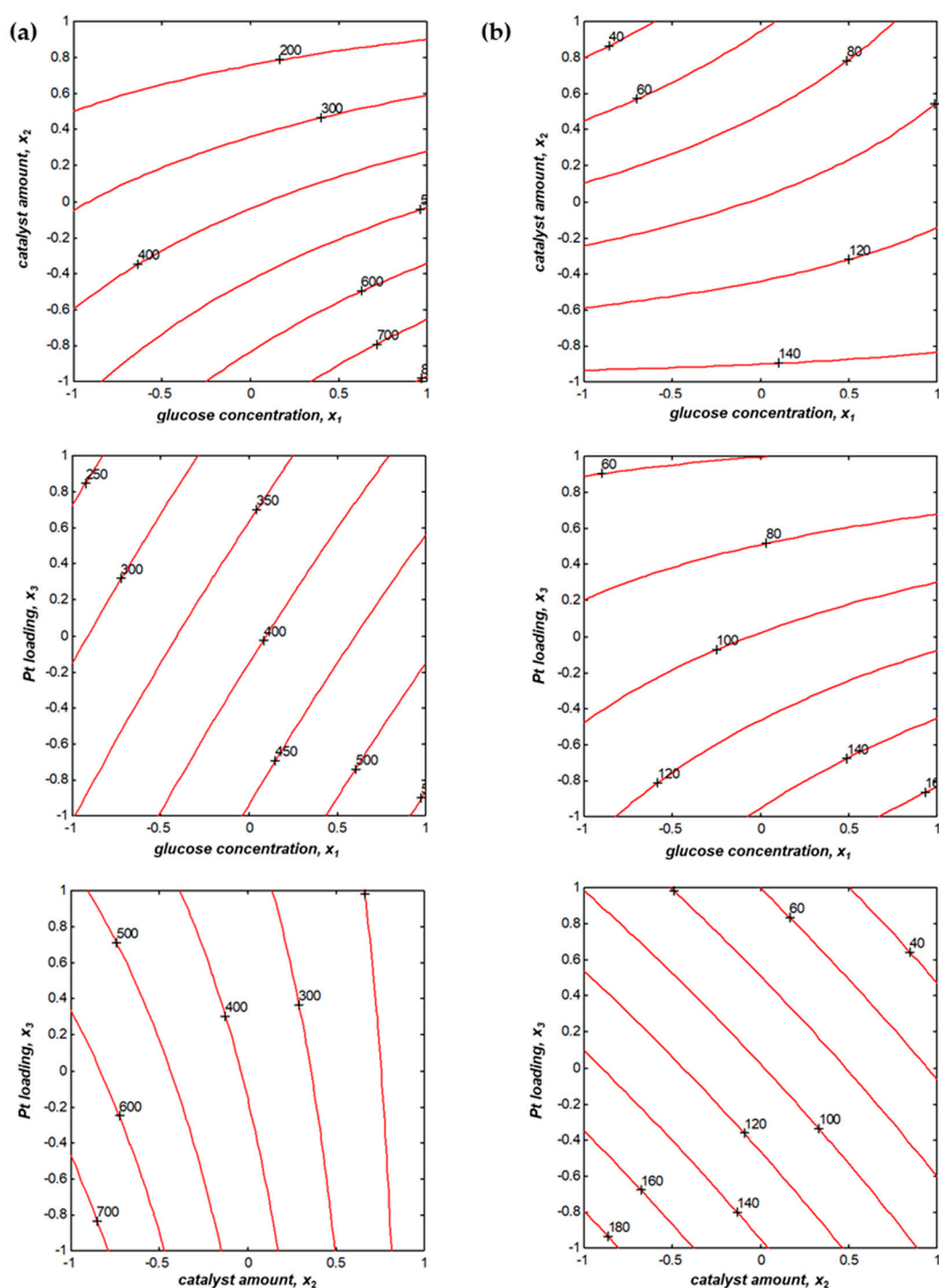


Figure 2. Response surfaces obtained by Matlab[®] elaboration for (a) DMASnBr₃/g-C₃N₄ and (b) PEA₂SnBr₄/g-C₃N₄ (for level codes −1 +1 see Table 1); the number close to each curve represents the HER.

The models elaborated on the experimental results are:

$$\text{HER} = 390 + 99x_1 - 251x_2 - 64x_3 - 70x_1x_2 - 6x_1x_3 + 60x_2x_3 \quad (2)$$

$$\text{HER} = 101 + 15x_1 - 43x_2 - 41x_3 + 14x_1x_2 - 12x_1x_3 + 4x_2x_3 \quad (3)$$

for DMASnBr₃/g-C₃N₄ and PEA₂SnBr₄/g-C₃N₄, respectively.

As apparent from the significance of the coefficients (Figure 1), the picture is similar for both composites, as the three variables affect significantly the HER ($p < 0.001$), although glucose concentration to a minor extent for $\text{PEA}_2\text{SnBr}_4/\text{g-C}_3\text{N}_4$ ($p < 0.01$); in particular, the photoreaction is favored by high glucose concentration and low levels of catalyst in the suspension and metal photodeposited on the catalyst surface. In addition, some interactions are statistically relevant, in particular x_1-x_2 and x_2-x_3 for $\text{DMASnBr}_3/\text{g-C}_3\text{N}_4$. In line with the response surfaces (see Figure 2), HER increases by keeping the catalyst amount at the low level but with the highest concentration of sacrificial agent, whereas both catalyst and co-catalyst at the lowest level enhance H_2 evolution. For $\text{PEA}_2\text{SnBr}_4/\text{g-C}_3\text{N}_4$, x_1-x_2 and x_1-x_3 are significative ($p < 0.01$ and $p < 0.05$, respectively); accordingly, the response surfaces show that also in this case, HER is maximized with low Pt loading and catalyst amount, and the high level of sacrificial biomass is useful, especially when working with 0.5 wt% Pt.

These findings can be explained considering that at low sacrificial substrate concentration, the mass transfer of glucose from water to the catalyst surface is the bottleneck of photocatalytic reaction, whilst in concentrated solutions, interfacial reactions govern the process, due to the saturation of glucose on the catalyst [17]. Furthermore, excessive Pt loading reduces the catalytic surface available for light absorption; additionally, a high concentration of suspended powder causes scattering of the incident radiation, thus decreasing the overall process [15,18].

Based on these outcomes, the selected conditions were 0.2 M glucose, 0.5 g L^{-1} catalyst, and 0.5 wt% Pt. These are advantageous, involving the use of small amounts of both catalyst and metal co-catalyst, and suggesting that large sample dilution could be avoided when using food industry wastewaters, where the total sugar content is up to tens of grams per liter [5].

The reproducibility was good, with relative standard deviations (RSD) $\leq 11\%$ and $\leq 15\%$ observed on four independent experiments for $\text{DMASnBr}_3/\text{g-C}_3\text{N}_4$ and $\text{PEA}_2\text{SnBr}_4/\text{g-C}_3\text{N}_4$, correspondingly.

For the best performing composite, $\text{DMASnBr}_3/\text{g-C}_3\text{N}_4$, the optimal conditions were further confirmed by validation of the model, working at the test point ($x_1 = 0$; $x_2 = 0$; $x_3 = 0$). Being the mean HER ($407 \pm 69 \mu\text{moles g}^{-1} \text{ h}^{-1}$, $p = 0.05$, $n = 4$) not significantly different from the value predicted by Equation (1), viz. $390 \mu\text{moles g}^{-1} \text{ h}^{-1}$, it is demonstrated that the model is effective and it can be applied to the whole experimental domain.

The chemometric study provided key information. First, it enabled pointing out the most convenient conditions for H_2 evolution, which resulted in a three-fold increase in HER relative to the first pilot work [13]; at the same time, the results collected clearly highlight the superior photocatalytic activity of $\text{DMASnBr}_3/\text{g-C}_3\text{N}_4$.

Given the very small difference between the MHPs' band gaps—2.85 and 2.74 eV for DMASnBr_3 and $\text{PEA}_2\text{SnBr}_4$, respectively [12,13]—and the higher surface area of $\text{PEA}_2\text{SnBr}_4/\text{g-C}_3\text{N}_4$ ($5.5 \text{ m}^2 \text{ g}^{-1}$ vs. $3.4 \text{ m}^2 \text{ g}^{-1}$ of $\text{DMASnBr}_3/\text{g-C}_3\text{N}_4$), it could be speculated that the better performance of the first catalyst derives from the different band alignments of the MHPs' valence band (VB) and conduction band (CB) edges with those of carbon nitride (gathered in Figure 3). This results in a different electron transfer and charge carriers stabilization mechanism.

The synergistic effect between the two constituents of the DMASnBr_3 -based photocatalyst, which works as a Z-scheme heterojunction, has been explained in terms of favorable band alignment and prolonged charge carrier lifetimes [13]. In the case of $\text{PEA}_2\text{SnBr}_4$, this is also true, but it is known that 2D perovskites have higher excitonic binding energies that may slightly reduce the charge carrier dynamics, thus affording a lower photocatalytic efficiency [21].

Another reason rationally stands in the better dispersibility of the DMA composite in aqueous phase due to its lower hydrophobicity. Because of the low surface area of the composites, good mechanical stirring is important; on the other hand, the fast sedimentation of the powders can be an advantage to recover them from water after photocatalysis.

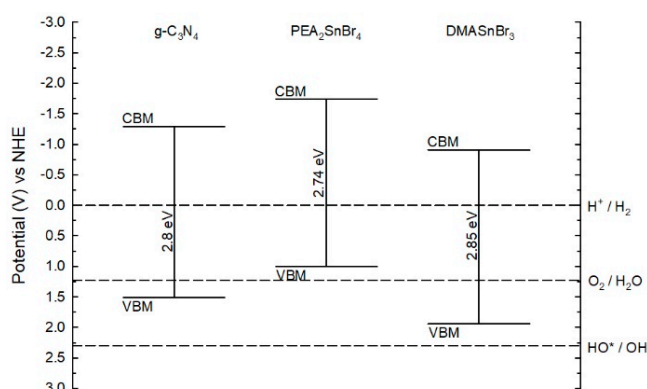


Figure 3. Scheme of the redox potentials (pH 7 vs NHE) of relevant reactions in relation to the band edges positions of as-prepared $g\text{-C}_3\text{N}_4$ and metal halide perovskites (MHPs).

2.2. Further Investigation of $\text{DMASnBr}_3/g\text{-C}_3\text{N}_4$

The photocatalytic behavior of the composite containing the DMASnBr_3 perovskite was further studied. Table 3 summarizes the HERs collected by key tests aimed at assessing the role of the metal co-catalyst, of the glucose biomass and to evaluate the contribute of “direct water splitting”, i.e., H_2 evolved from water in the absence of the sacrificial donor [22].

Table 3. Key experiments for evaluating the photocatalytic system based on 33% $\text{DMASnBr}_3/g\text{-C}_3\text{N}_4$ (simulated solar light).

Sample	HER ($\mu\text{moles g}^{-1} \text{h}^{-1}$) ¹
water + 0.5 g L ⁻¹ catalyst	12
water + 0.5 g L ⁻¹ catalyst + 0.5 wt% Pt	62
0.2 M glucose + 0.5 g L ⁻¹ catalyst	142
0.2 M glucose + 0.5 g L⁻¹ catalyst + 0.5 wt% Pt	925
water	n.q.
0.2 M glucose	n.q.

¹ RSDs $\leq 11\%$ ($n = 3$); n.q.; not quantifiable ($<0.008 \mu\text{moles h}^{-1}$).

As is apparent, the model biomass has a major role in sustaining H_2 evolution, which is 15-fold higher relative to the HER observed in neat water (the contribution of “direct water splitting” is $<7\%$). In addition, the metal co-catalyst largely rules the photoreaction to give gas-phase H_2 , both in the presence of the sacrificial agent and in pure water. Notice that appreciable HER was gained also with no metal, underlining the potentiality of such photoactive material. This evidence corroborates a photoreaction mechanism typical of the photocatalytic systems for H_2 production from water [1,3,23], wherein:

(1) The catalyst absorbs the radiation generating the characteristic charge separation (holes and electrons);

(2) The sacrificial organic material serves as scavenger of the oxidizing species and, by undergoing gradual oxidation (photoreforming), supplies electrons;

(3) The metal works as an electron collector and is the active site for hydrogen ions reduction while hindering charge carriers’ recombination and backward reactions [3].

Regarding the $\text{DMASnBr}_3/g\text{-C}_3\text{N}_4$ composite, valence band holes—not hydroxyl radicals in the solution—are generated in $g\text{-C}_3\text{N}_4$ and these trigger biomass oxidation to boost H_2 formation from water, while avoiding a complete aqueous phase reforming of the organic substrate until mineralization [1], which instead occurs in titanium dioxide photocatalysis, especially with Pd co-catalyst [16,22,24]. The negligible H_2 evolution ($<0.008 \mu\text{moles h}^{-1}$) observed by irradiation of neat water and 0.2 M glucose, as the control tests (Table 3), further substantiated the proposed mechanism.

The synergistic effect between carbon nitride and perovskite described above and assessed in foregoing work [13] was here confirmed in glucose solution under the best conditions. Indeed, HER was 74 and 40 $\mu\text{moles g}^{-1} \text{h}^{-1}$ for $\text{g-C}_3\text{N}_4$ and DMASnBr_3 individually tested, respectively, against 925 $\mu\text{moles g}^{-1} \text{h}^{-1}$ of the hybrid catalyst (see Table 3).

The values of apparent quantum yield (AQY), calculated as the percent ratio H_2 moles/incident photons moles [5] and turn over number (TON), calculated as the ratio H_2 moles/Pt moles [16], for $\text{DMASnBr}_3/\text{g-C}_3\text{N}_4$ in the optimized conditions are reported in Table 4.

Table 4. Apparent quantum yield (AQY) and turn over number (TON) values for $\text{DMASnBr}_3/\text{g-C}_3\text{N}_4$ (0.5 g L^{-1} catalyst, 0.5 wt% Pt).

Sample	AQY	TON	HER ($\mu\text{moles g}^{-1} \text{h}^{-1}$)
distilled water	0.1	202	62
aqueous glucose	2.0	3007	925
aqueous starch	0.3	473	146

These results are very interesting and highlight the efficiency of the composite catalyst that, despite the very low surface area ($<4 \text{ m}^2 \text{ g}^{-1}$, 18-times lower than that of the commercial nanometric P25 TiO_2 [25]), promoted HER equal to about one third of the latter ($2906 \mu\text{moles g}^{-1} \text{h}^{-1}$), under the same conditions. To point out the role of surface area and to provide comparable data, we tested a lower amount of P25 TiO_2 (0.028 g L^{-1}) to have approximately the same catalytic surface area of 0.5 g L^{-1} of the composite. HER was $377 \mu\text{moles g}^{-1} \text{h}^{-1}$, 2.5-times lower than that afforded by employing the composite.

Additional trials were devoted to investigate the stability of the catalyst upon subsequent irradiations. As is shown in Figure 4, no loss of efficiency was noticed using the recycled powder in a new sample solution, and only a 25% decrease in H_2 evolution in a third treatment.

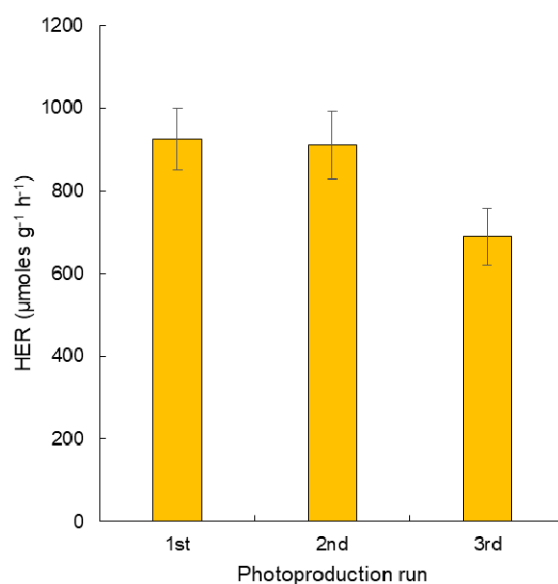


Figure 4. Reusability of $\text{DMASnBr}_3/\text{g-C}_3\text{N}_4$ (0.5 g L^{-1} , 0.5 wt% Pt, 0.2 M aqueous glucose), RSD < 11% ($n = 3$).

The X-ray diffraction (XRD) profiles overlaid in Figure 5 attest the preservation of the pristine structure in the composite employed after the three sequential photoreactions (18 h total irradiation time) in aqueous glucose.

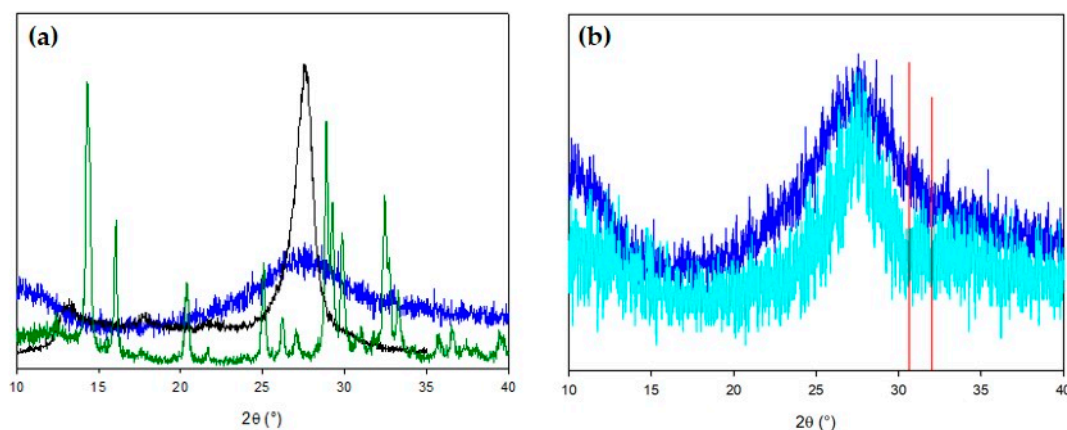


Figure 5. XRD patterns collected on (a) DMASnBr₃ (green), g-C₃N₄ (black) and as-prepared DMASnBr₃/g-C₃N₄ (blue); (b) the composite after three irradiations (azure) compared to the as-prepared one (blue) and reference metallic tin (red).

Although in the XRD pattern of the as-synthesized catalyst the fingerprints of the perovskite are not visible, a broad signal centered on the principal peak of the carbon nitride that stabilizes an amorphous structure of the perovskite is present, as previously discussed [13]. Superimposable patterns were observed on both fresh and recycled materials (see Figure 5b); moreover, no peaks related to metallic Sn were found after catalysis (instead observed working in TEOA solution, data not shown). These findings support both the integrity of the hybrid material and the maintenance of the perovskite in the photocatalyst. Thus, this can be utilized for at least three consecutive irradiations, as a proof of photo-chemical stability that strengthens the applicability of DMASnBr₃/g-C₃N₄ for a potential practical use.

Such new outcomes prompted us to test the composite in the presence of a polysaccharide sacrificial substance, and starch was chosen as the representative bio-polymer because of its low cost, large availability and attractiveness as bio-oxygenated for H₂ photogeneration [5,24].

Hydrogen gas was effectively produced from starch solution (see Table 4), at a concentration of 4.5 g L⁻¹ (the maximum solubility [5]), although at lower amount compared to glucose. This is justified considering that the rate of hydrogen evolution from water decreases with increasing molecular weights and structure complexity of carbohydrates [15–17,24]. Additionally, since the VB holes are the oxidizing species of the present catalytic system, an intimate contact between the sacrificial substrate and the catalyst surface is certainly required. This could be more favored with monosaccharides than polysaccharides with a branched skeleton such as starch, which realistically has slower mass transfer kinetics from solution to the composite surface sites [16,24].

Such new findings highlight that DMASnBr₃/g-C₃N₄ is able to carry forward H₂ photoproduction exploiting the sacrificial role of a raw polysaccharide such as soluble starch, which thus can be employed directly without any pre-treatment, e.g., enzymatic hydrolysis or microwave-assisted hydroxylation [26,27].

3. Materials and Methods

Preparation and characterization of the two new composites 5% PEA₂SnBr₄/g-C₃N₄ and 33% DMASnBr₃/g-C₃N₄ was reported by these authors in very recent works [12,13].

Surface area measurements were carried out by the Brunauer, Emmett and Teller (B.E.T.) single point method using a Flowsorb II 2300 (Micromeritics, Norcross, GA, USA) apparatus. The sample was accurately weighed and degassed at 80 °C for 1.5 h, under a continuous stream of a N₂-He (30:70) mixture, and then it was put in liquid nitrogen for gas adsorption. Evonik Aeroxide® P25 TiO₂ (10–50 nm, 60.8 m² g⁻¹ [25]) was supplied by Evonik Industries AG (Hanau, Germany). H₂ evolution experiments were conducted in distilled water containing 0.025–0.2 M glucose (99.9%, Carlo Erba

Reagents) or 4.5 g L⁻¹ soluble starch (ACS reagent, Carlo Erba Reagents), irradiated in Pyrex glass containers [28]. After addition of the catalyst (0.028, 0.5, 2 g L⁻¹), the suspension was deoxygenated by Ar bubbling (20 min) and irradiated for 6 h, under magnetic stirring. When using Pt as the co-catalyst, chloroplatinic acid (H₂PtCl₆, 38% Pt basis) from Sigma-Aldrich (Milan, Italy) was employed as the metal source. Since Pt is in situ photodeposited on the catalyst surface, after Ar bubbling, a small volume from an H₂PtCl₆ aqueous solution (0.15, 3 or 15 g L⁻¹) was added using a 10–100 µL micropipette to the catalyst suspension, directly in the photoreactor. This was closed with sleeve stopper septa and was irradiated, as described in the following, achieving simultaneous Pt deposition and H₂ production [23,28–30]. Irradiation was done under simulated solar light using a Solar Box 1500e (CO.FO.ME.GRA S.r.l., Milan, Italy) set at a power factor of 500 W m⁻², and equipped with UV outdoor filter made of IR-treated soda lime glass. The apparent photon flux, measured as previously described [5], was 1.53 × 10⁷ photons moles s⁻¹. The headspace H₂ was quantified by gas chromatography coupled with thermal conductivity detection (GC-TCD) [28]. The results obtained relative to H₂ evolution are shown in the paper as micromoles of gas per gram of catalyst per hour (µmoles g⁻¹ h⁻¹, HER). Reproducibility was appraised on the RSD% from four independent photoproduction runs. For catalyst recycling tests, the catalyst was recovered by filtration (0.45 µm nylon membrane), washed with plenty of distilled water, left drying at room temperature for several weeks in the dark, and finally re-used under the optimized conditions. Room temperature Cu-radiation XRD spectra were acquired by a Bruker D8 diffractometer (Billerica, MA, USA).

4. Conclusions

Lab-scale tests proved the superior photocatalytic activity of DMASnBr₃/g-C₃N₄ against PEA₂SnBr₄/g-C₃N₄ for H₂ evolution from glucose solution, under simulated solar light, using Pt as a co-catalyst. The systematic optimization of the experimental conditions by a DoE provided HER higher than 900 µmoles g⁻¹ h⁻¹ using the former composite. The results herein collected highlight the importance to work under selected conditions to maximize the H₂ yield while reducing the use of catalyst and co-catalyst. The comparison with P25 TiO₂ strengthened the catalytic efficiency of DMASnBr₃/g-C₃N₄, while avoiding the handling of nano-sized powders. Notably, a rewarding H₂ formation (around 140 µmoles g⁻¹ h⁻¹) was gained, also avoiding any metal deposition. DMASnBr₃/g-C₃N₄ showed good photochemical stability to be utilized for two consecutive runs without any loss of efficiency and with a decrease of 25% in the third cycle, as verified by H₂ evolution measurement and XRD analysis. The system turned out to work also in raw starch solution as sustainable, model sacrificial biomass, providing ca. 150 µmoles g⁻¹ h⁻¹. These outcomes corroborate the potential application of this new class of photocatalysts for clean energy retrieval under sustainable conditions and deserve further investigation to move the photoproduction experiments on sugar-rich wastewaters under natural solar light.

Author Contributions: Conceptualization, A.S., L.M. and A.P.; validation, A.S. and A.P.; formal analysis, A.S.; investigation, A.S. and L.R.; data curation, A.S.; writing—original draft preparation, A.S.; writing—review and editing, L.M., D.D. and A.P.; visualization, A.S. and L.R.; supervision, A.S. and A.P.; funding acquisition, A.P. All authors have read and agreed to the published version of the manuscript.

Funding: This research received no external funding.

Acknowledgments: The Authors acknowledge Giuseppina Sandri (Department of Drug Sciences, University of Pavia) for surface area measurements.

Conflicts of Interest: The authors declare no conflict of interest.

References

1. Wen, J.; Xie, J.; Chen, X.; Li, X. A review on g-C₃N₄-based photocatalysts. *Appl. Surf. Sci.* **2017**, *391*, 72–123. [[CrossRef](#)]
2. Nasir, M.S.; Yang, G.; Ayub, I.; Wang, S.; Wang, L.; Wang, X.; Yan, W.; Peng, S.; Ramakarishna, S. Recent development in graphitic carbon nitride based photocatalysis for hydrogen generation. *Appl. Catal. B* **2019**, *257*, 117855. [[CrossRef](#)]
3. Lam, S.S.; Nguyen, V.-H.; Dinh, M.T.N.; Khieu, D.Q.; La, D.D.; Nguyen, H.T.; Vo, D.V.N.; Xia, C.; Varma, R.S.; Shokouhimehr, M.; et al. Mainstream avenues for boosting graphitic carbon nitride efficiency: Towards enhanced solar light-driven photocatalytic hydrogen production and environmental remediation. *J. Mater. Chem. A* **2020**, *8*, 10571–10603. [[CrossRef](#)]
4. Speltini, A.; Scalabrini, A.; Maraschi, F.; Sturini, M.; Pisanu, A.; Malavasi, L.; Profumo, A. Improved photocatalytic H₂ production assisted by aqueous glucose biomass by oxidized g-C₃N₄. *Int. J. Hydrogen Energy* **2018**, *43*, 14925–14933. [[CrossRef](#)]
5. Speltini, A.; Gualco, F.; Maraschi, F.; Sturini, M.; Dondi, D.; Malavasi, L.; Profumo, A. Photocatalytic hydrogen evolution assisted by aqueous (waste)biomass under simulated solar light: Oxidized g-C₃N₄ vs. P25 titanium dioxide. *Int. J. Hydrogen Energy* **2019**, *44*, 4072–4078. [[CrossRef](#)]
6. Zhang, L.; Zhang, J.; Xia, Y.; Xun, M.; Chen, H.; Liu, X.; Yin, X. Metal-free carbon quantum dots implant graphitic carbon nitride: Enhanced photocatalytic dye wastewater purification with simultaneous hydrogen production. *Int. J. Mol. Sci.* **2020**, *21*, 1052. [[CrossRef](#)]
7. Huang, H.; Pradhan, B.; Hofkens, J.; Roeffaers, M.B.; Steele, J.A. Solar-driven metal halide perovskite photocatalysis: Design, stability, and performance. *ACS Energy Lett.* **2020**, *5*, 1107–1123. [[CrossRef](#)]
8. Romani, L.; Malavasi, L. Solar-driven hydrogen generation by metal halide perovskites: Materials, approaches, and mechanistic view. *ACS Omega* **2020**, (in press). [[CrossRef](#)]
9. Stanks, S.D.; Snaith, H.L. Metal-halide perovskites for photovoltaic and light-emitting devices. *Nat. Nanotec.* **2015**, *10*, 391–402.
10. Pu, Y.-C.; Fan, H.-C.; Liu, T.-W.; Chen, J.-W. Methylamine lead bromide perovskite/protonated graphitic carbon nitride nanocomposites: Interfacial charge carrier dynamics and photocatalysis. *J. Mater. Chem. A* **2017**, *5*, 25438–25449. [[CrossRef](#)]
11. Li, Z.; Wu, S.; Zhang, J.; Yuan, Y.; Wang, Z.; Zhu, Z. Improving photovoltaic performance using perovskite/surface-modified graphitic carbon nitride heterojunction. *Sol. RRL* **2020**, *4*, 1900413. [[CrossRef](#)]
12. Romani, L.; Bala, A.; Kumar, V.; Speltini, A.; Milella, A.; Fracassi, F.; Listorti, A.; Profumo, A.; Malavasi, L. PEA₂SnBr₄: A water-stable lead-free two-dimensional perovskite and demonstration of its use as co-catalyst in hydrogen photogeneration and organic-dye degradation. *J. Mater. Chem. C* **2020**, *8*, 9189–9194. [[CrossRef](#)]
13. Romani, L.; Speltini, A.; Ambrosio, F.; Mosconi, E.; Profumo, A.; Marelli, M.; Margadonna, S.; Milella, A.; Fracassi, F.; Listorti, A.; et al. Water-stable DMASnBr₃ lead-free perovskite for effective solar-driven photocatalysis. *Angew. Chem. Int. Ed.* **2020**. [[CrossRef](#)]
14. Pisanu, A.; Speltini, A.; Quadrelli, P.; Drera, G.; Sangaletti, L.; Malavasi, L. Enhanced air-stability of Sn-based hybrid perovskites induced by dimethylammonium (DMA): Synthesis, characterization, aging and hydrogen photogeneration of the MA_{1-x}DMA_xSnBr₃ system. *J. Mater. Chem. C* **2019**, *7*, 7020–7026. [[CrossRef](#)]
15. Leung, D.Y.C.; Fu, X.; Wang, C.; Ni, M.; Leung, M.K.H.; Wang, X.; Fu, X. Hydrogen production over titania based photocatalysts. *ChemSusChem* **2010**, *3*, 681–694. [[CrossRef](#)]
16. Silva, C.G.; Sampaio, M.J.; Marques, R.R.N.; Ferreira, L.A.; Tavares, P.B.; Silva, A.M.T.; Faria, J.L. Photocatalytic production of hydrogen from methanol and saccharides using carbon nanotube-TiO₂ catalysts. *Appl. Catal. B Environ.* **2015**, *178*, 82–90. [[CrossRef](#)]
17. Fu, X.; Long, J.; Wang, X.; Leung, D.Y.C.; Ding, Z.; Wu, L.; Zhang, Z.; Li, Z.; Fu, X. Photocatalytic reforming of biomass: A systematic study of hydrogen evolution from glucose solution. *Int. J. Hydrogen Energy* **2008**, *33*, 6484–6491. [[CrossRef](#)]
18. Kisch, H. On the problem of comparing rates or apparent quantum yields in heterogeneous photocatalysis. *Angew. Chem. Int. Ed.* **2010**, *49*, 9588–9589. [[CrossRef](#)] [[PubMed](#)]
19. Speltini, A.; Sturini, M.; Maraschi, F.; Dondi, D.; Serra, A.; Profumo, A.; Buttafava, A.; Albini, A. Swine sewage as sacrificial biomass for photocatalytic hydrogen gas production: Explorative study. *Int. J. Hydrogen Energy* **2014**, *39*, 11433–11440. [[CrossRef](#)]

20. Speltini, A.; Sturini, M.; Maraschi, F.; Dondi, D.; Fisogni, G.; Annovazzi, E.; Profumo, A.; Buttafava, A. Evaluation of UV-A and solar light photocatalytic hydrogen gas evolution from olive mill wastewater. *Int. J. Hydrogen Energy* **2015**, *40*, 4303–4310. [[CrossRef](#)]
21. Baranowski, M.; Plochocka, P. Excitons in metal-halide perovskites. *Adv. Energy Mater.* **2020**, *10*, 1903659. [[CrossRef](#)]
22. Bowker, M. Photocatalytic hydrogen production and oxygenate photoreforming. *Catal. Lett.* **2012**, *142*, 923–929. [[CrossRef](#)]
23. Zhang, J.-H.; Wei, M.-J.; Wei, Z.-W.; Pan, M.; Su, C.-Y. Ultrathin graphitic carbon nitride nanosheets for photocatalytic hydrogen evolution. *ACS Appl. Nano Mater.* **2020**, *3*, 1010–1018. [[CrossRef](#)]
24. Kennedy, J.; Bahruji, H.; Bowker, M.; Davies, P.R.; Bouleghlimat, E.; Issarapanacheewin, S. Hydrogen generation by photocatalytic reforming of potential biofuels: Polyols, cyclic alcohols, and saccharides. *J. Photochem. Photobiol. Chem.* **2018**, *356*, 451–456. [[CrossRef](#)]
25. Jiang, X.; Manawan, M.; Feng, T.; Qian, R.; Zhao, T.; Zhou, G.; Kong, F.; Wang, Q.; Dai, S.; Pan, J.H. Anatase and rutile in evonik aeroxide P25: Heterojunctioned or individual nanoparticles? *Catal. Today* **2018**, *300*, 12–17. [[CrossRef](#)]
26. Li, K.L.; Xia, L.X.; Li, J.; Pang, J.; Cao, G.Y.; Xi, Z.W. Salt-assisted acid hydrolysis of starch to D-glucose under microwave irradiation. *Carbohydr. Res.* **2001**, *331*, 9–12.
27. Wang, D.; Hou, F.; Ma, X.; Chen, W.; Yan, L.; Ding, T.; Ye, X.; Liu, D. Study on the mechanism of ultrasound-accelerated enzymatic hydrolysis of starch: Analysis of ultrasound effect on different objects. *Int. J. Biol. Macromol.* **2020**, *148*, 493–500. [[CrossRef](#)] [[PubMed](#)]
28. Speltini, A.; Sturini, M.; Dondi, D.; Annovazzi, E.; Maraschi, F.; Caratto, V.; Profumo, A.; Buttafava, A. Sunlight-promoted photocatalytic hydrogen gas evolution from water-suspended cellulose: Systematic study. *Photochem. Photobiol. Sci.* **2014**, *13*, 1410–1419. [[CrossRef](#)]
29. Pisanu, A.; Speltini, A.; Vigani, B.; Ferrari, F.; Mannini, M.; Calisi, N.; Cortigiani, B.; Caneschi, A.; Quadrelli, P.; Profumo, A.; et al. Enhanced hydrogen photogeneration by bulk g-C₃N₄ through a simple and efficient oxidation route. *Dalton Trans.* **2018**, *47*, 6772–6778. [[CrossRef](#)]
30. Sun, H.; Zhou, X.; Zhang, H.; Tu, W. An efficient exfoliation method to obtain graphitic carbon nitride nanosheets with superior visible-light photocatalytic activity. *Int. J. Hydrogen Energy* **2017**, *42*, 7930–7937. [[CrossRef](#)]

Publisher's Note: MDPI stays neutral with regard to jurisdictional claims in published maps and institutional affiliations.



© 2020 by the authors. Licensee MDPI, Basel, Switzerland. This article is an open access article distributed under the terms and conditions of the Creative Commons Attribution (CC BY) license (<http://creativecommons.org/licenses/by/4.0/>).